Draft version October 9, 2019
Preprint typeset using LaTeX style emulateapj v. 08/13/06

SPECTROSCOPIC ORBITS OF SUBSYSTEMS IN MULTIPLE STARS. VI.

Andrei Tokovinin
Cerro Tololo Inter-American Observatory, Casilla 603, La Serena, Chile
Draft version October 9, 2019

ABSTRACT

Thirteen spectroscopic orbits of late-type stars are determined from the high-resolution spectra taken with the CHIRON echelle spectrometer at the 1.5-m CTIO telescope. Most (HIP 14194B, 40523A, 41171A, 51578A, 57572B, 59426A, 62852B, 66438A, 87813B, and 101472A) are inner subsystems in hierarchical multiple stars with three or four components. The periods range from 2.2 to 1131 days. Masses of the components, orbital inclinations, and projected rotation velocities are estimated, the presence or absence of the lithium line is noted. In addition to those systems, HIP 57021 is a simple 54-day twin binary, and HIP 111598 is a compact triple-lined system with periods of 5.9 and 271 days. This object is likely old, but, nevertheless, the secondary component in the inner pair does not rotate synchronously with the orbit. The period-eccentricity diagram of 528 known inner low-mass spectroscopic subsystems (including 36 from this paper series) is given. The distribution of the inner periods is smooth, without any details around the tidal circularization period of $\sim$10 d.
Subject headings: binaries:spectroscopic, binaries:visual

1. INTRODUCTION

Spectroscopic orbits of close binaries belonging to hierarchical stellar systems are determined here, continuing the series of similar papers (Tokovinin 2016a,b, 2018b,c, 2019). The current collection of data on stellar hierarchies, MSC (Tokovinin 2018a), contains many spectroscopic binaries with yet unknown orbits. Ongoing work slowly fills this gap.

The systems studied here are listed in Table 1. The data are collected from Simbad and *Gaia* DR2, the radial velocities (RVs) are mostly determined here. The first column gives the WDS-style (Mason et al. 2001) code based on the J2000 coordinates (most stars are indeed present in the WDS). The HIP and HD identifiers, spectral types, photometric and astrometric data refer either to the individual stars or to the unresolved close subsystems.

The structure of this paper is similar to the previous ones. The data and methods are briefly recalled in Section 2, where the orbital elements are also given. Then each system is discussed in Section 3. The paper closes with a short summary in Section 4.

2. OBSERVATIONS AND DATA ANALYSIS

2.1. *Spectroscopic observations*

The spectra used here were taken with the 1.5 m telescope sited at the Cerro Tololo Inter-American Observatory (CTIO) in Chile and operated by the SMARTS Consortium.[1] The observing time (20 hours per semester) was allocated through NOAO. Observations were made with the CHIRON optical echelle spectrograph (Tokovinin et al. 2013) by the telescope operators in service mode. The RVs are determined from the cross-correlation function (CCF) of echelle orders with the binary mask based on the solar spectrum, as detailed in (Tokovinin 2016a). The RVs derived by this method should be on the absolute scale if the wavelength calibration is accurate. The CHIRON RVs were checked against standards and a small offset of +0.15 km s^{-1} was found in Tokovinin (2018b); it is not applied to the RVs given here. The RV errors depend on the width and contrast of the CCF dip, presence of other dips, signal to noise ratio, and other factors. The rms residuals from the orbits can be as low as 0.03 km s^{-1}, but typically are between 0.1 and 0.2 km s^{-1} for the systems studied here. We assign the RV errors (hence weights) to match roughly the residuals, with larger errors assigned to blended or noisy dips.

The CCF contains two dips in the case of double-lined systems. The dip width is related to the projected rotation velocity $V \sin i$, while its area depends on the spectral type, metallicity, and relative flux. Table 2 lists average parameters of the Gaussian curves fitted to the CCF dips. It gives the number of averaged measurements N (blended CCFs were not used), the dip amplitude a, its dispersion σ, the product $a\sigma$ proportional to the dip area (hence to the relative flux), and the projected rotation velocity $V \sin i$, estimated from σ by the approximate formula given in (Tokovinin 2016a) and valid for $\sigma < 12$ km s^{-1}. The last column indicates the presence or absence of the lithium 6708Å line in individual components.

2.2. *Orbit calculation*

As in the previous papers of this series, orbital elements and their errors were determined by the least-squares fits with weights inversely proportional to the adopted errors. The IDL code `orbit`[2] was used (Tokovinin 2016c). It can fit spectroscopic, visual, or combined visual/spectroscopic orbits. Formal errors of orbital elements are determined from these fits. The elements of spectroscopic orbits are given in Table 3, in standard notation. Its last column contains the masses $M \sin^3 i$ for double-lined binaries. For single-lined systems, the mass of the primary star (listed here with colons) is estimated from its absolute V magnitude, and the minimum

Electronic address: atokovinin@ctio.noao.edu
[1] http://www.astro.yale.edu/smarts/

[2] Codebase: http://www.ctio.noao.edu/~atokovin/orbit/ and https://doi.org/10.5281/zenodo.61119

TABLE 1
Basic parameters of observed multiple systems

WDS (J2000)	Comp.	HIP	HD	Spectral type	V (mag)	$V-K$ (mag)	μ^*_α (mas yr^{-1})	μ_δ	RV (km s^{-1})	ϖ^{a} (mas)
03030−0205	A	14194	18795	F7V	6.33	1.18	104	6	35.3	17.40
	B	...	...	K3V?	9.97	2.66	108	2	36.12	17.61
08164−0314	A	40523	69351	F8	7.25	1.39	−109	12	28.53	12.82
	B	...	...	...	10.39	...	−94	−6	29.90	11.16
08240−1548	AB	41171	70904	F2/F3V	8.55	1.06	−26	−15	−1.43	6.61
10321−7005	A	51578	91561	F5V:	9.05	1.02	−9	2	−3.89	7.85
	B	...	...	...	9.33	1.11	−9	3	−4.2	7.85
11414−4101	A	57021	101614	G0V	6.87	1.46	166	−124	16.37	28.80
11480−6607	A	57572	102579	K1V+...	8.33	1.76	−268	172	10.6:	26.95
	B	...	...	K6.5V	9.11	2.36	−279	165	14.14	26.74
12114−1647	A	59426	105913	K1	7.05	1.70	−152	−47	2.37	29.67
	B	...	...	...	8.69	...	−152	−47	2.1	29.39
12530+1502	A	62852	111959	F5	7.93	0.46	−24	29	−8.1	6.17
	B	...	...	...	8.65	1.12	−24	29	−8.05	6.52
13372−6142	AB	66438	118261	F6V	5.63	1.20	147	−120	21.13	27.99[b]
17563−1549	A	87813	163336	A1V	5.89	0.19	−1	−73	−24.0	12.38
	B	...	...	...	8.89	1.18	1	−65	−9.24	15.64
20339−2710	A	101472	195719	G8V	9.38	1.77	71	−84	−89.87	11.75
	B	...	...	...	11.97	2.89	71	−87	−89.5	11.86
22366−0034	AB	111598	214169	G0III	8.38	1.99	13	−41	18.20	6.85

[a]Proper motions and parallaxes are taken from the *Gaia* DR2 (Gaia collaboration 2018), where available.
[b]*Hipparcos* parallax (van Leeuwen 2007).

TABLE 2
CCF parameters

HIP	Comp.	N	a	σ (km s^{-1})	$a\sigma$ (km s^{-1})	$V \sin i$ (km s^{-1})	Li 6708Å
14194	Ba	5	0.258	4.588	1.182	5.5	N
14194	Bb	5	0.201	4.656	0.934	5.7	N
40523	Aa	5	0.158	4.162	0.659	4.3	Y
40523	Ab	5	0.151	4.455	0.672	5.2	Y
40523	B	5	0.014	3.168	0.043	0.0	...
41171	Aa	17	0.023	16.912	0.380	30:	Y?
41171	Ab	17	0.060	5.371	0.321	7.5	Y?
51578	Aa	8	0.057	14.601	0.833	26:	N
51578	B	2	0.035	24.050	0.853	43:	N
57021	Aa	12	0.167	3.474	0.579	1.3	Y
57021	Ab	12	0.167	3.468	0.579	1.2	Y
57572	A	2	0.522	3.629	1.894	2.3	N
57572	Ba	12	0.234	4.522	1.056	5.4	N
57572	Bb	12	0.190	4.484	0.852	5.3	N
59426	Aa	10	0.270	4.587	1.238	5.5	Y
59426	Ab	10	0.161	3.742	0.604	2.8	N
59426	B	3	0.504	4.345	2.188	4.9	N
62852	Ba	9	0.119	5.052	0.612	6.7	Y
62852	Bb	9	0.103	5.624	0.577	8.1	Y
66438	Aa	8	0.119	3.712	0.441	2.7	Y
66438	Ab	8	0.073	3.455	0.252	1.1	Y
66438	B	8	0.061	7.687	0.471	12.4	N?
87813	Ba	1	0.206	7.183	1.476	11.4	Y
87813	Bb	1	0.030	5.998	0.178	8.9	Y?
101472	Aa	9	0.290	3.489	1.011	1.4	N
101472	Ab	9	0.148	3.587	0.529	2.1	N
111598	Aa	24	0.049	15.608	0.771	27:	N
111598	Ab	24	0.061	4.227	0.258	4.5	N
111598	B	24	0.044	3.562	0.158	1.9	N

mass of the secondary that corresponds to the 90° inclination is derived from the orbit. Table 4, published in ful electronically, provides individual RVs. The *Hipparcos* number of the primary star and the system identifier (components joined by comma) in the first two columns define the pair. Then follow the Julian date, the RV, its adopted error σ (blended CCF dips are assigned large errors), and the residual to the orbit (O−C). The last column specifies to which component this RV refers ('a' for the primary, 'b' for the secondary, 'c' for the tertiary of HIP 111598). The RVs of other visual components are provided, for completeness, in Table 5. It contains the HIP number, the component letter, the Julian date, and the RV.

2.3. *Gaia DR2 astrometry*

Rich data contained in the second *Gaia* data release, DR2 (Gaia collaboration 2018), contribute to the study

TABLE 3
Spectroscopic orbits

HIP	System	P (d)	T (JD +24,00,000)	e	$\omega_{\rm A}$ (deg)	K_1 (km s^{-1})	K_2 (km s^{-1})	γ (km s^{-1})	rms$_{1,2}$ (km s^{-1})	$M_{1,2}\sin^3 i$ ($\mathcal{M}_\odot$)
14194	Ba,Bb	1136	58180.6	0.575	281.0	10.027	10.241	36.121	0.16	0.27
		±5.8	±3.7	±0.023	±2.1	±0.356	±0.363	±0.062	0.18	0.27
40523	Aa,Ab	28.9577	58427.130	0.524	228.0	48.994	49.088	28.531	0.12	0.87
		±0.0004	±0.005	±0.001	±0.1	±0.065	±0.065	±0.038	0.13	0.87
41171	Aa,Ab	25.4160	58449.990	0.533	308.1	46.739	48.325	−1.438	1.67	0.70
		±0.0011	±0.007	±0.001	±0.2	±0.683	±0.068	±0.043	0.17	0.67
51578	Aa,Ab	2.19189	58300.390	0.078	237.1	40.087	...	−3.891	0.33	1.30:
		±0.00001	±0.012	±0.004	±2.0	±0.132	...	±0.087	...	>0.34
57021	Aa,Ab	53.6806	58498.043	0.462	55.9	33.930	33.906	16.371	0.03	0.60
		±0.0029	±0.0034	±0.002	±0.4	±0.098	±0.098	±0.041	0.03	0.60
57572	Ba,Bb	36.40406	58315.672	0.142	122.5	35.463	36.337	14.143	0.06	0.68
		±0.0020	±0.046	±0.001	±0.5	±0.052	±0.081	±0.027	0.21	0.67
59426	Aa,Ab	211.585	58383.709	0.281	284.0	15.484	17.706	2.369	0.13	0.38
		±0.029	±0.270	±0.002	±0.5	±0.0039	±0.039	±0.020	0.08	0.33
62852	Ba,Bb	13.9288	58195.404	0.4324	207.6	66.903	67.747	−8.050	0.10	1.30
		±0.0001	±0.002	±0.0005	±0.01	±0.056	±0.056	±0.023	0.07	1.28
66438	Aa,Ab	8.0714	58554.569	0	0	58.158	67.131	21.131	0.07	0.88
		±0.0002	±0.0012	fixed	fixed	±0.043	±0.043	±0.025	0.10	0.76
87813	Ba,Bb	728.96	53759.40	0.500	135.3	10.453	16.306	−9.244	0.21	0.57
		±0.79	±9.11	±0.038	±1.1	±0.754	±1.874	±0.341	0.37	0.37
101472	Aa,Ab	354.88	58243.32	0.397	12.2	18.485	20.541	−89.867	0.04	0.89
		±0.05	±0.13	±0.001	±0.1	±0.025	±0.026	±0.010	0.05	0.80
111598	A,B	271.21	58560.65	0.230	306.3	14.224	29.777	18.199	...	1.49
		±0.21	±0.78	±0.005	±0.9	±0.132	±0.239	±0.037	0.26	0.71
111598	Aa,Ab	5.86806	58383.4927	0	0	67.484	71.379	...	0.86	0.84
		±0.00003	±0.0007	fixed	fixed	±0.335	±0.072	...	0.24	0.79

TABLE 4
Radial velocities and residuals (fragment)

HIP	System	Date (JD +24,00,000)	RV	σ (km s^{-1})	(O−C)	Comp.
14194	Ba,Bb	56922.7662	27.13	0.20	−0.10	a
14194	Ba,Bb	56922.7662	45.13	0.20	−0.07	b
14194	Ba,Bb	56937.7094	27.04	0.20	−0.15	a
14194	Ba,Bb	56937.7094	45.30	0.20	0.06	b

TABLE 5
Radial velocities of other components

HIP	Comp.	Date (JD +24,00,000)	RV (km s^{-1})
40523	B	58228.4952	29.936
40523	B	58232.4856	30.119
40523	B	58454.7632	30.203
40523	B	58456.7519	29.369
40523	B	58484.7321	29.885
40523	B	58513.6322	30.078
40523	B	58526.6080	29.707
51578	B	58194.6145	−4.2:
51578	B	58195.6229	−3.7:
57572	A	58193.7407	10.658
57572	A	58195.6377	10.456
62852	A	58194.7057	−5.4:
62852	A	58195.7036	−6.4:
66438	B	58559.6566	21.199
66438	B	58565.7035	21.227
66438	B	58578.7043	21.213
66438	B	58581.8054	21.233
66438	B	58583.7687	21.184
66438	B	58594.7517	21.169
66438	B	58668.6582	20.987
66438	B	58699.5444	21.214

of multiple stars in various ways. Here I use the potential of detecting astrometric subsystem by the difference of the short-term proper motion (PM) measured by *Gaia* with the long-term PM $\mu_{\rm mean}$ deduced from the comparison between the *Gaia* and *Hipparcos* positions (Brandt 2018). The long-term PM is very accurate. A statistically significant difference $\Delta\mu_{\rm DR2-mean}$ indicates presence of an astrometric subsystems with period from a few years to a few decades.

3. INDIVIDUAL OBJECTS

For each observed system, the corresponding Figure shows a typical CCF (the Julian date and individual components are marked on the plot) together with the RV curve representing the orbit. In the RV curves, squares denote the primary component, triangles denote the secondary component, while the full and dashed lines plot the orbit. Masses of stars are estimated from absolute magnitudes, orbital periods of wide pairs from their projected separations (see Tokovinin 2018a). Some results of speckle interferometry at the Southern Astrophysical Research Telescope (SOAR) are used (Tokovinin et al. 2019).

3.1. *HIP 14194 (Triple)*

The outer visual pair STF 341 was discovered by W. Struve in 1831. Its estimated period is ∼8 kyr; the system turned by 9° during 188 yrs since its discovery at a constant separation of $8\farcs7$. The *Gaia* parallaxes and PMs of both components A and B match perfectly; the star A is located on the main sequence, while B is above it. There is no significant $\Delta\mu_{\rm DR2-mean}$. The star A was targeted by exo-planet RV surveys.

The double-lined nature of B has been discovered with CHIRON (Tokovinin 2015). Here its spectroscopic orbit with a period of 3.1 yr is determined (Figure 1). The period and parallax correspond to the semimajor axis of

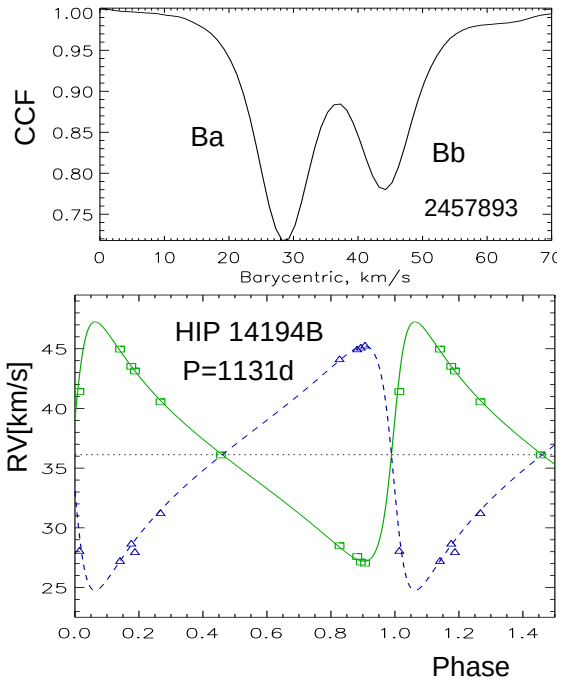

FIG. 1.— CCF (top) and RV curve (bottom) of HIP 14194 Ba,Bb. In this and the following Figures, the upper panel shows a typical CCF, with the Julian date of the observation indicated. The lower panel presents the phased RV curve where the full lines and squares denote the orbit and RVs of the primary component, the dashed line and triangles refer to the secondary component.

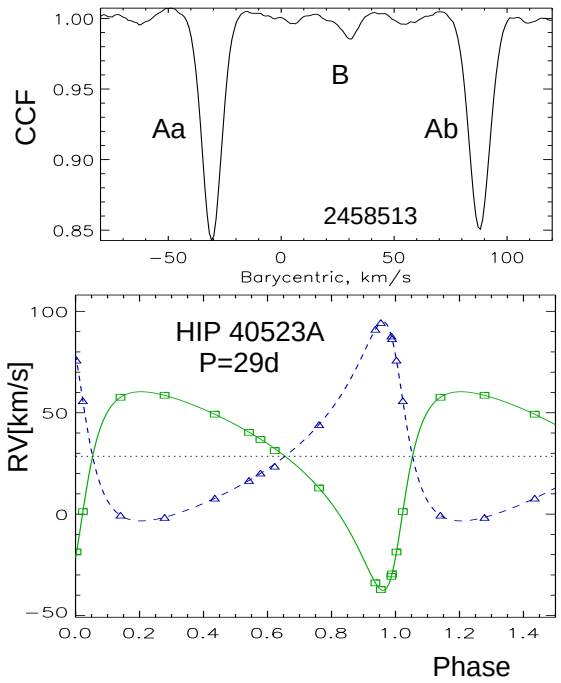

FIG. 2.— CCF (top) and RV curve (bottom) of HIP 40523 Aa,Ab.

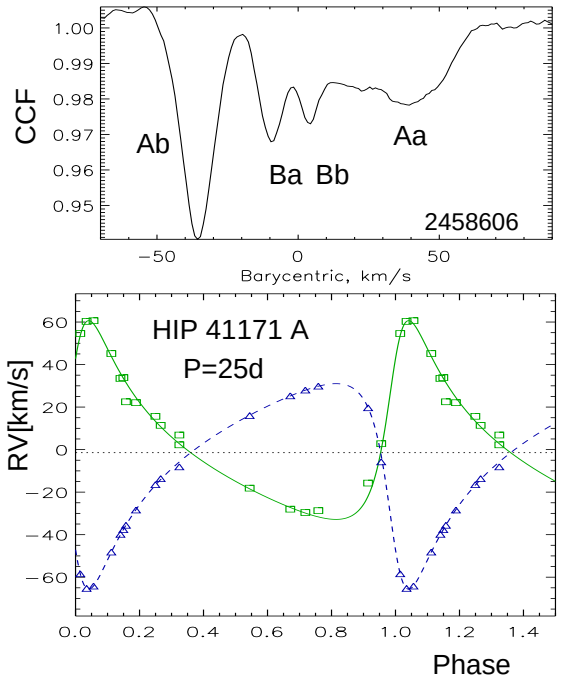

FIG. 3.— CCF (top) and RV curve (bottom) of HIP 41171 Aa,Ab.

43 mas, making the Ba,Bb pair accessible to speckle interferometry. Indeed, it has been resolved at SOAR in 2018 at similar separation and shows an orbital motion in agreement with the short period. The speckle measurements combined with the RVs lead to the preliminary visual elements $a = 41$ mas, $\Omega = 162°$, $i = 139°$. The masses of Ba and Bb are 0.76 and 0.74 $M_\odot$ and their sum, 1.49 $M_\odot$, is similar to the estimated mass of the component A, 1.22 $M_\odot$. The orbital inclination of Ba,Bb evaluated from the spectroscopic masses is 45° or 135°; the latter agrees with the provisional visual elements.

3.2. *HIP 40523 (Triple)*

The outer 1.″4 visual pair A,B (HWE 21, ADS 6707), known since 1879, has an estimated period of ∼600 yr and has turned only by 21° since its discovery. The companion B is fainter than A by 3.5 mag and its RV is barely measurable from the weak dip in the CCF; the mean RV(B) and the rms scatter are 29.90 and 0.29 km s^{-1}, respectively. On the other hand, the dips belonging to the inner binary Aa,Ab are strong and equal. Its double-lined nature was discovered by Nordström et al. (2004). The orbit of this pair determined here has $P = 28.96$ d and $e = 0.524$ (Figure 2). The mass ratio $q = 0.998$ makes the inner pair a perfect twin. The estimated masses of Aa and Ab are 1.29 $M_\odot$, hence the inclination is $i_{\rm Aa,Ab} = 62°$. Considering the detectable lithium line and the kinematics typical of a young disk population, $(U, V, W) = (-43.0, -9.9 - 23.1)$ km s^{-1}, this system could be relatively young.

3.3. *HIP 41171 (Quadruple)*

The outer visual binary A,B discovered by R. A. Rossiter in 1940 (RST 4396) has a separation of 1″ and an estimated period of ∼1 kyr. The magnitude difference between A and B is moderate, about 2 mag. All available photometry and astrometry, including *Gaia*, refers to the unresolved pair AB. Understandably, there is no significant $\Delta\mu$ because the outer period is too long and the inner period too short for detecting an astrometric acceleration.

Nordström et al. (2004) discovered that the pair contains a double-lined spectroscopic subsystem and the stars are slightly metal deficient, [Fe/H]=−0.2 dex. Our first observations revealed CCFs with three dips belong-

ing to Aa, Ab, and B. The dip of Aa is wide and shallow owing to its fast axial rotation, while the dips of Ab and B are much sharper. However, further monitoring revealed that the component B is also a double-lined binary: its dip separated in two components Ba and Bb, with a slow change of RVs (Figure 3). The orbital period of Ba,Bb exceeds one year, and observations will continue in the next season, selecting dates when the dips of Aa and Ab do not overlap with the dips of B. I do not report here the RVs of B and the parameters of its CCF dips. The area of the blended dip of Ba+Bb is used to derive relative fluxes.

The RV of A is measured poorly and its residuals from the orbit are large, so the elements of Aa,Ab are based mostly on the accurate RVs of Ab. Although the dip areas of Aa, Ab, and B are comparable, the actual relative fluxes differ more substantially because spectral lines are stronger in cool stars. Adopting effective temperatures of 6500, 6400, and 5900 K for Aa, Ab, and B, respectively, I estimate their individual V magnitudes as 9.41, 9.65, and 10.39 mag. The resulting $\Delta V_{\rm AB} = 1.61$ mag is a little less than $\Delta Hp_{\rm A,B} = 1.65$ mag from *Hipparcos* and $\Delta I_{\rm A,B} = 1.8$ mag from SOAR speckle interferometry. The absolute magnitudes of Aa and Ab match main-sequence masses of 1.28 and 1.23 $M_\odot$ (spectral types F5V and F6V), in agreement with the measured mass ratio $q_{\rm Aa,Ab} = 0.97$. The resulting orbital inclination of the Aa,Ab pair is $i_{\rm Aa,Ab} \approx 54°$. These estimates are only preliminary.

Considering the likely presence of a weak lithium lines in the spectra of Aa and Ab and the measurable rotation of these stars, the system can be relatively young. The faster rotation of Aa can be explained by its earlier spectral type, hence a shallower convective zone and a longer braking time compared to Ab.

3.4. *HIP 51578 (Triple)*

The outer 7.″8 binary HJ 4335, discovered by J. Hershel in 1834, has an estimated period of ∼20 kyr. The stars A and B are almost equal, $\Delta V = 0.29$ mag, and are located on the main sequence. The component A has no significant $\Delta\mu$. The RV of B measured by CHIRON (-4.2 and -3.7 km s^{-1}) and *Gaia* (-2.9 km s^{-1}) is close to the center-of-mass RV of A, -3.4 km s^{-1}. Owing to the fast rotation of B, its RVs are not accurate.

The RV of A is variable, as established by Nordström et al. (2004). The period is short, $P = 2.192$ d, but the orbit is definitely non-circular, $e = 0.078 \pm 0.004$ (Figure 4). One RV measured by Desidera et al. (2006) can be fitted by a slight adjustment of the period, but this increases the residuals substantially, from 0.33 km s^{-1} to 0.75 km s^{-1}. Ongoing tidal circularization of an eccentric orbit with a slight decrease in period offers potential explanation for the deviant RV.

I used the ASAS-3 photometry in the V band (Pojmanski 1997)[3] to search for photometric signal with the orbital period. The components A and B are measured jointly. The plot in Figure 5 shows the residual rms variation after subtracting the best-fitting sine and cosine terms at each trial frequency. The strongest feature is found at the frequency of 0.4137 day^{-1} (period 2.417 d); it implies an rms variation of only 3.22 mmag and may

[3] http://www.astrouw.edu.pl/asas/?page=catalogues

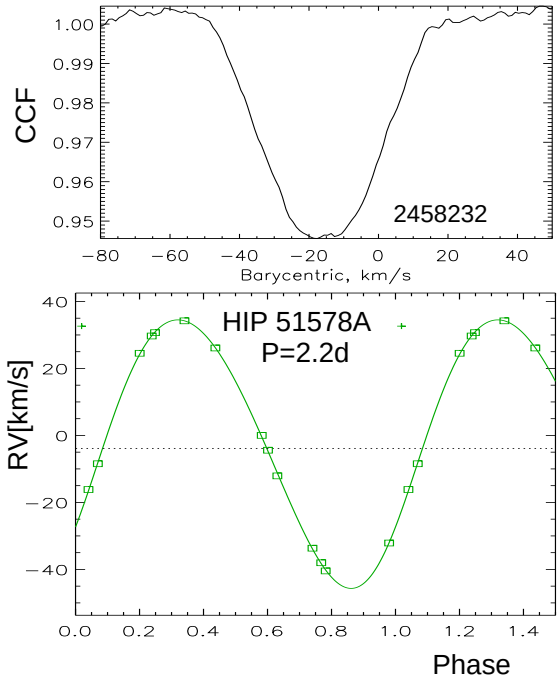

FIG. 4.— CCF (top) and RV curve (bottom) of HIP 51578 Aa,Ab. The cross shows RV from Desidera et al. (2006), not used to fit the elements.

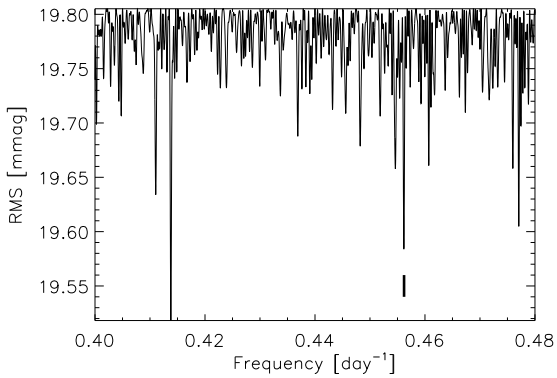

FIG. 5.— Periodogram of HIP 51578 AB. The orbital frequency of 0.4562 day^{-1} is marked by the thick line. The strongest dip is at 0.4137 day^{-1}.

correspond to the rotation of the star B. There are also dips at the orbital frequency and at its alias, possibly caused by the starspots synchronized with the orbit of Aa,Ab. The ASAS photometry proves the absence of eclipses in the subsystem.

The minimum mass of the spectroscopic secondary Ab is 0.34 $M_\odot$. The projected rotation $V \sin i$ for Aa and B estimated crudely from the width of the CCF dips, 26 and 43 km s^{-1} respectively, agrees with 25.1 and 39.4 km s^{-1} measured by Desidera et al. (2006). The synchronous rotation speed of a star of 1.3 $R_\odot$ radius is 29.7 km s^{-1}, hence the orbital inclination of Aa,Ab is ∼60° and the actual mass of Ab is about 0.4 $M_\odot$.

3.5. *HIP 57021 (Binary)*

This is just a nearby (35 pc) spectroscopic binary belonging to the 67-pc sample of solar-type stars (Tokovinin 2014). Double lines were detected by Nordström et al. (2004), but the orbital period remained unknown. The components are practically indistinguishable: the mass

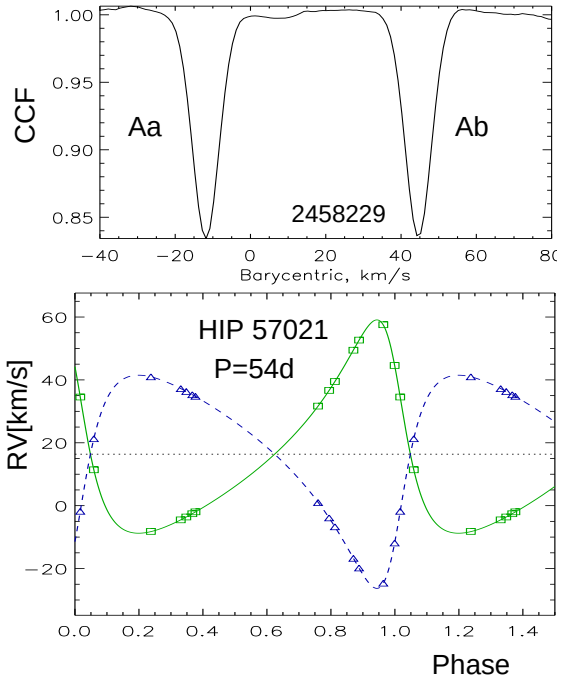

FIG. 6.— CCF (top) and RV curve (bottom) of HIP 57021.

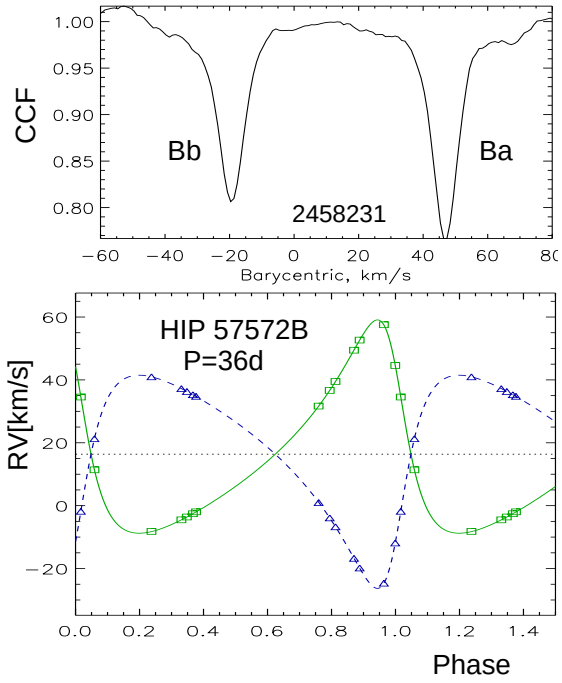

FIG. 7.— CCF (top) and RV curve (bottom) of HIP 57572 Ba,Bb.

ratio is 1.0007±0.0042 and the dips are equal. The period of this perfect twin is 53.7 days, well above the tidal circularization limit. Note the small residuals of 0.03 km s^{-1}. The orbital inclination is $i \approx 60°$. The projected axial rotation is very slow, $V \sin i \approx 1.3$ km s^{-1}. Nevertheless, lithium is not yet destroyed in the atmosphere of these G0V dwarfs and they are featured in the catalogs of chromospherically active stars (e.g. Boro Saikia et al. 2018). The kinematics does not distinguish this star from the disk population, $(U, V, W) = (31.6, 6.6, -11.0)$ km s^{-1}. Fuhrmann & Chini (2019) measured the metallicity [Fe/H]=−0.41 dex. Brandt (2018) did not detect any significant acceleration which, together with very small RV residuals, indicates the absence of additional components with periods less than ∼30 yr.

3.6. *HIP 57572 (Quadruple)*

This is a low-mass nearby (37 pc) stellar system with a fast PM. The outer 8.″2 binary GLI 168 was first resolved in 1852. Its period is ∼3.5 kyr. The secondary star B, 1.4 mag fainter than A, is a double-lined spectroscopic binary (Nordström et al. 2004). Here its orbit with $P =$ 36 d is determined (Figure 7). This is yet another twin with $q = 0.976$. The masses of Ba and Bb estimated from their absolute magnitudes, ∼0.7 $M_\odot$, are close to the spectroscopic masses $M \sin^3 i$, hence the orbit of Ba,Bb is seen edge-on.

Nordström et al. (2004) measured the mean RV(A) of 8.8 km s^{-1} and found it to be variable by 1.9 km s^{-1} over a 2-yr period. The variability is confirmed by the different RVs measured with CHIRON, 10.5 km s^{-1}, and *Gaia*, 12.8 km s^{-1} (the latter with a large error of 1.8 km s^{-1}), and by the difference with the center-of-mass RV of B, 14.14 km s^{-1}. Therefore, A likely contains a low-mass satellite with yet unknown period. An indirect evidence of the existence of a subsystem is the large error of the DR2 parallax of A, 0.3 mas, while the parallax of B is measured by *Gaia* with an error of 0.03 mas. There

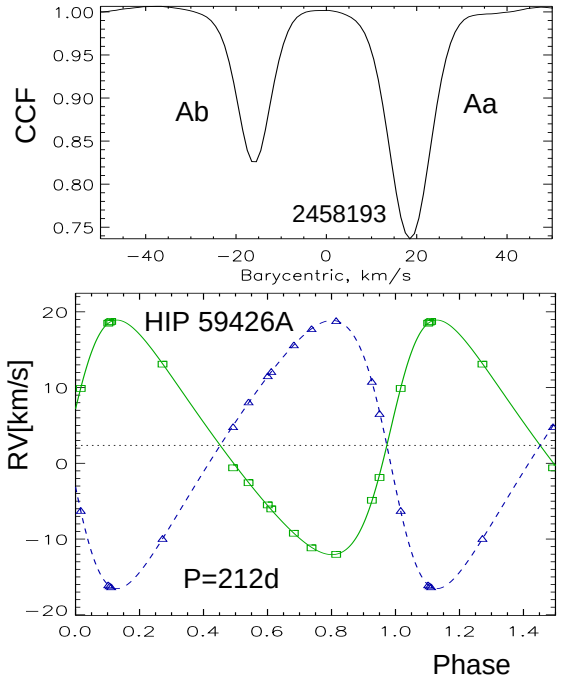

FIG. 8.— CCF (top) and RV curve (bottom) of HIP 59426 Aa,Ab.

is a small acceleration $\Delta\mu_{\rm DR2-mean} \approx 2$ mas yr^{-1}. The observed motion of the pair A,B may show a wave caused by the subsystem Aa,Ab.

3.7. *HIP 59426 (Triple)*

Like the previous object, this system is a nearby (34 pc) triple K-dwarf with a fast PM. The outer pair A,B was first measured in 1877 at 6.″9 (S 634, ADS 8444) and has closed down to 4.″7 since. Its estimated period is 1.2 kyr. Double lines in the spectrum of A were noted by Nordström et al. (2004). Monitoring with CH-

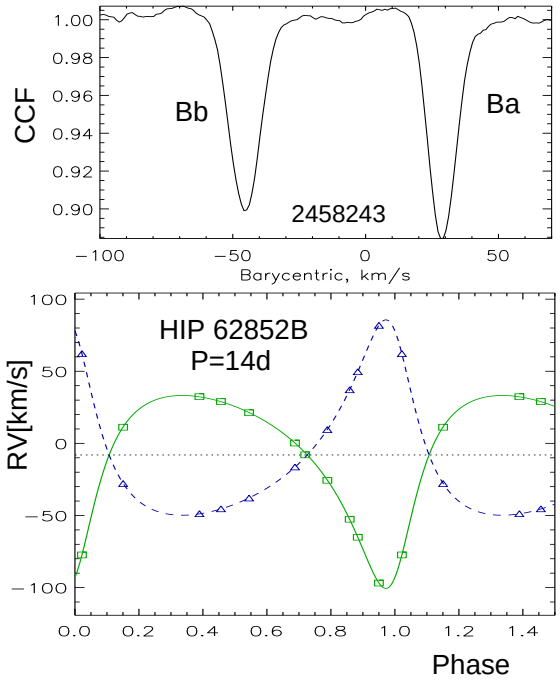

FIG. 9.— CCF (top) and RV curve (bottom) of HIP 62852 Ba,Bb.

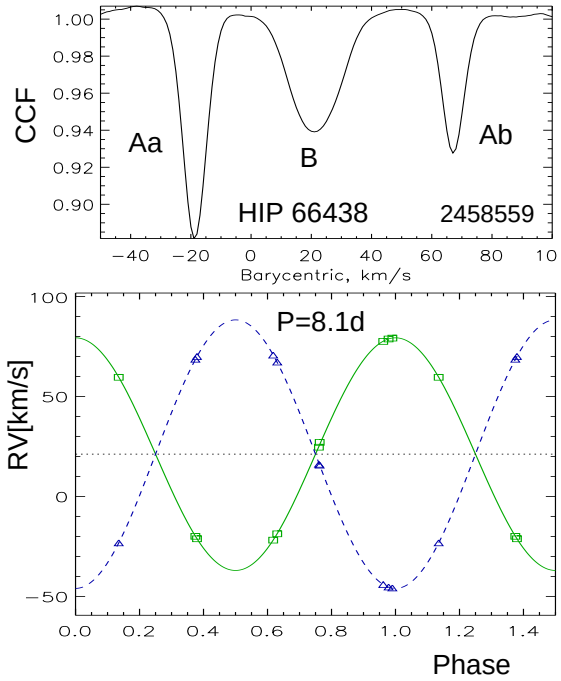

FIG. 10.— CCF (top) and RV curve (bottom) of HIP 66438 Aa,Ab.

IRON, started in 2015, revealed a relatively long period, $P = 212$ d, and a mass ratio $q = 0.874$ (Figure 8). The estimated semimajor axis of the inner orbit is 27 mas. The subsystem Aa,Ab was resolved in 2018 and 2019 by speckle interferometry at SOAR at similar separations, just under the formal diffraction limit. The astrometric acceleration $\Delta\mu_{\rm DR2-mean} = (-5.90, -0.2)$ mas yr^{-1} possibly results from the orbital motion of Aa,Ab. On the other hand, the PM difference between A and B matches the observed relative motion of the outer pair with the average velocity of 21 mas yr^{-1} (or 3.4 km s^{-1}) in the plane of the sky.

Interestingly, the lithium 6708Å line is securely detected in the spectra of Aa and is equally securely missing in both Ab and B. As lithium destruction depends on both age and mass, this datum can help in establishing the age of this system. Its spatial velocity $(U, V, W) = (-17.4, -17.4, -7.3)$ km s^{-1} is close to the motion of young stars in the solar vicinity, such as the TW Hya group. However, the orbital motion of A in the wide pair has not been subtracted from the calculated space velocity.

3.8. *HIP 62852 (Quadruple)*

This is 2+2 quadruple system where two close pairs revolve around a common center on a wide orbit with an estimated period of 13 kyr. The outer 5.″7 visual pair STF 1686 (ADS 8693) has been discovered by W. Struve in 1823. However, its first measurement is misleadingly inaccurate and leaves an impression that the pair moves too fast. *Gaia* establishes the physical nature of the outer pair beyond any doubt. The WDS lists another faint companion D at 1.″88 from A, but it is not detected by *Gaia*, so I assume that D is just a background star.

The component A was resolved by speckle interferometry into a 0.″12 pair Aa,Ab (YSC 215) with an estimated period of ∼60 yr. The visual secondary, B, is a double-lined pair reported by Nordström et al. (2004). Here its spectroscopic orbit with $P = 13.9$ d and $q = 0.987$ is determined (Figure 9). Its estimated inclination is 80°. The spectra of Ba and Bb have the lithium line, and these stars rotate slightly faster than the pseudo-synchronous speed.

3.9. *HIP 66438 (Triple)*

This is a bright (HR 5113) and nearby (36 pc) tight triple system. The outer visual pair A,B (I 365AB) was discovered by R. T. A. Innes in 1900. Its orbit with a period of 35.0 yr is of high quality (grade 2). The distant component C listed in the WDS is optical. The spectroscopic subsystem has been discovered by Evans (1968); Fekel (1981); Fuhrmann & Chini (2019) by the presence of triple lines in the spectrum. The latter authors estimated the masses of the components as 1.21, 1.19, and 1.09 $M_\odot$ and noted the presence of the lithium lines in Aa and Ab. I confirm this finding; on the other hand, the lithium line in the spectrum of B can be only guessed. The presence of lithium and a relatively fast axial rotation of B (12.4 km s^{-1}) suggest youth and are in tension with the age of 2.3 Gyr estimated by Fuhrmann & Chini (2019). Relative areas of the CCF dips correspond to $\Delta m_{\rm A,B} = 0.42$ mag in the outer pair, while WDS gives $\Delta m_{\rm A,B} = 0.60$ mag, confirmed by the speckle interferometry at SOAR. The spectroscopic pair certainly belongs to the brighter visual component A.

Our circular orbit with a period of 8.07 d corresponds to the masses $M \sin^3 i$ of 0.88 and 0.76 $M_\odot$. An attempt to fit an eccentric orbit does not improve the residuals and the resulting eccentricity of 0.003 is not significant, hence the circular orbit is imposed. The masses quoted above (which match the outer mass sum of 3.39 $M_\odot$ derived from the visual orbit and the *Hipparcos* parallax) yield the inner inclination of 64° or 117°. The inclination of the outer orbit is 117°, hinting at possible co-planarity. However, the outer orbit has a high eccentricity $e = 0.78$.

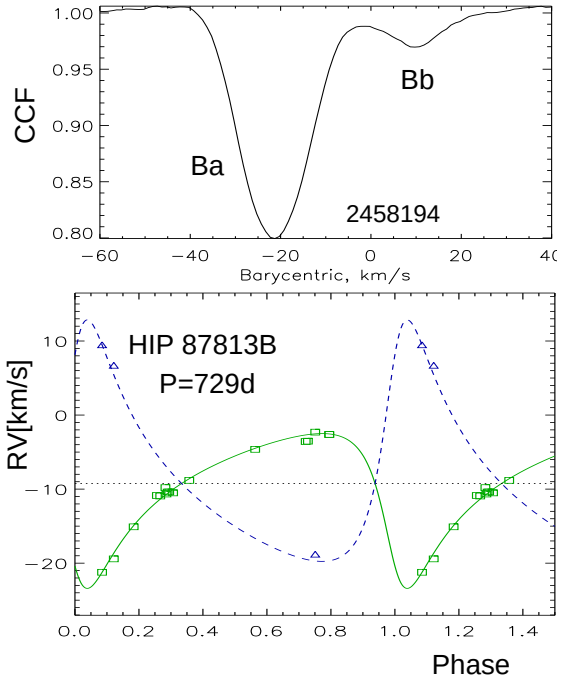

FIG. 11.— CCF (top) and RV curve (bottom) of HIP 87813 Ba,Bb.

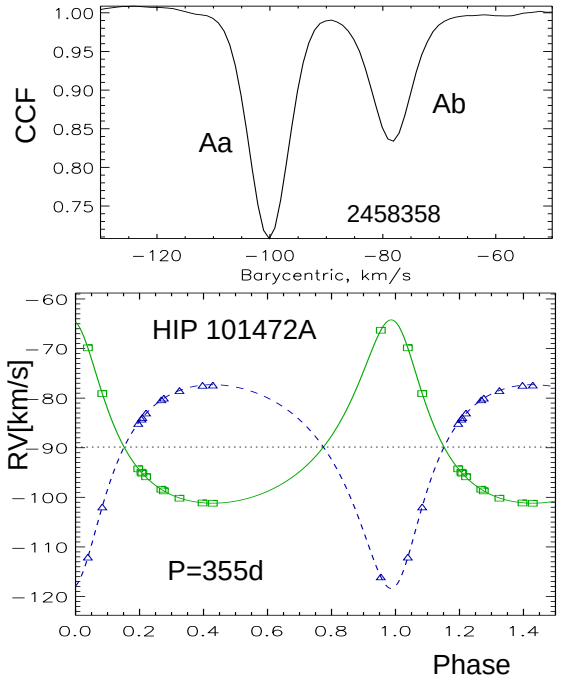

FIG. 12.— CCF (top) and RV curve (bottom) of HIP 101472 Aa,Ab.

The outer pair is presently near the apastron of its eccentric orbit. The mean RV(B) is 21.18 km s^{-1} (rms scatter 0.08 km s^{-1}), very close to the center of mass RV(A), 21.13 km s^{-1}. Further monitoring should reveal the RV variation of both A and B caused by the eccentric 35-yr outer orbit. The next periastron passage will be in 2037.

3.10. *HIP 87813 (Quadruple)*

This is a 2+2 quadruple system. The outer pair A,B (HJ 2814, ADS 10891) at 20.″6 separation is known since 1830; its estimated period is ∼30 kyr. The main component A (HR 6681), of A1V spectral type, has variable RV according to Nordstrom & Andersen (1985). The short-term PMs of A measured by both *Gaia* and *Hipparcos* differ significantly from the mean PM: $\Delta\mu_{\rm DR2-mean} = (-3.0, -1.5)$ mas yr^{-1} and $\Delta\mu_{\rm HIP2-mean} = (-5.3, +6.0)$ mas yr^{-1}. The period of the subsystem Aa,Ab is likely a few years.

The RV of the secondary component B (BD−15°4723, ADS 10891B) was found to be variable by Tokovinin & Smekhov (2002); a tentative orbit with $P = 761$ d based on those RVs was featured in the old versions of the MSC. Now, using additional RVs from CHIRON and Du Pont echelle (Tokovinin et al. 2015), a definitive orbit with $P = 729$ d is determined (Figure 11). Moreover, a weak dip produced by the secondary component Bb is detected, allowing to measure the mass ratio, $q_{\rm Ba,Bb} = 0.82$. The color and absolute magnitude of B correspond to a G0V star with a mass of 1.1 $M_\odot$. Estimated masses lead to the inclination of $i_{\rm Ba,Bb} \approx 53°$. The lithium line is present in the spectrum of Ba.

3.11. *HIP 101472 (Triple)*

In this triple system, the outer orbit has a long period of ∼200 kyr and a wide separation of 52″. The components A and B have common parallax, PM, and RV and are located on the main sequence. No astrometric acceleration of A can be detected.

Double lines in the component A were noted by Nordström et al. (2004) who estimated the mass ratio of 0.92. The star was observed with CHIRON since 2015, showing double CCF dips with slow variation. The orbit has a period close to one year and $q_{\rm Aa,Ab} = 0.92$ (Figure 12). Its semimajor axis is 14 mas, so the pair can be resolved by speckle interferometry at 8-m telescopes. The estimated inclination is $i_{\rm Aa,Ab} = 77°$. Presence of a 1-yr subsystem, unaccounted for by the *Gaia* DR2 astrometry, can bias the parallax, but this has not happened in this case. The spatial velocity $(U, V, W) = (-84.0, -51.2, 18.6)$ km s^{-1} and [Fe/H]=−0.23 dex indicate that the system may belong to the thick disk (note the relatively large systemic RV of −89.8 km s^{-1}); slow axial rotation and the absence of lithium support this view.

3.12. *HIP 111598 (Triple)*

Triple lines in the spectrum of this star were detected by Guillout et al. (2009) in the survey of X-ray sources. On JD 2452482.60693, they measured the RVs of 43 and 3 km s^{-1}, but do not indicate to which components they refer. High chromospheric activity and location well above the main sequence in the color-magnitude diagram (CMD) suggested that this system could be young. The photometric period of 5.827 days was found by Kiraga (2012); small amplitudes, 0.039 mag in the V band and 0.025 mag in the I band, indicate that the variability is caused by starspots.

The CHIRON spectra show triple lines, all with variable RVs (Figure 13, a). The weakest narrow lines, attributed here to the component B, move relatively slowly with a period of 271 days. The other two components Aa and Ab have stronger lines of unequal width and move much faster, with a period of 5.87 days. The elements of both orbits were fitted jointly using the `orbit3.pro`

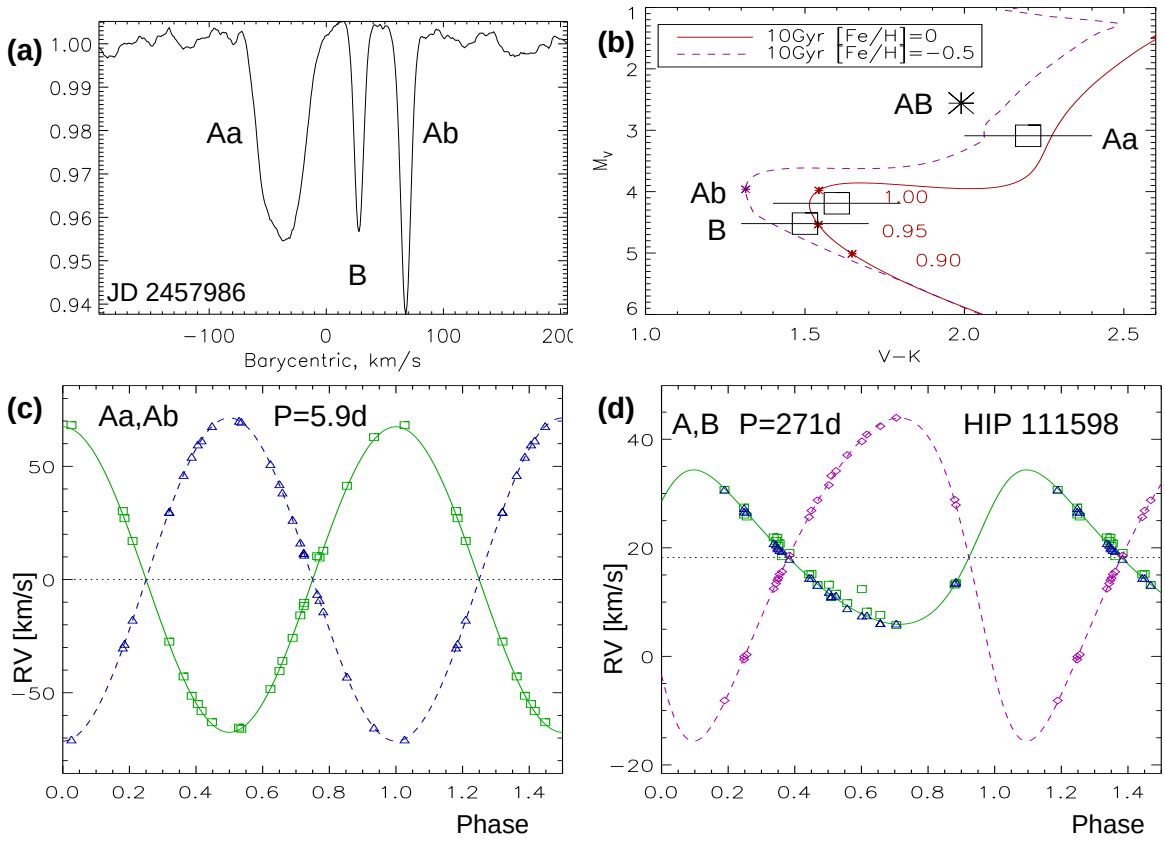

FIG. 13.— The triple system HIP 111598. (a) A typical CCF with a triple dip recorded on JD 2457986. (b) Approximate location of the components on the CMD. The 10-Gyr isochrones from Dotter et al. (2008) (asterisks mark the masses) are plotted (full line for solar metallicity, dashed line for [Fe/H]=−0.5). The large asterisk corresponds to the combined light of AB. (c) The RV curve of the inner pair Aa,Ab, with the outer orbit subtracted. (d) The RV curve of the outer pair A,B with the inner orbit subtracted. Squares, triangles, and diamonds refer to Aa, Ab, and B, respectively.

IDL code (Tokovinin & Latham 2017; Tokovinin 2017).[4] The weighted rms residuals for Aa, Ab, and B are 0.91, 0.23, and 0.24 km s^{-1}, respectively. The large residuals of Aa are explained by its wide CCF profile, likely distorted by starspots. Both orbits are plotted in Figure 13 (c,d). With the period ratio of 46, the interaction between the inner and outer pairs is not negligible. However, our observations obtained over a limited period of time are well represented by two Keplerian orbits with fixed elements. Detailed dynamical modeling of this system is outside the scope of this paper. The minimum component masses $M \sin^3 i$ are 0.835, 0.790 $M_\odot$ for the inner pair and 1.492, 0.712 for the outer orbit. The mass ratios of 0.947 and 0.476 define the relative masses of Aa, Ab, and B as 1:0.95:0.93.

A star of one solar radius rotating synchronously with the inner orbit would have an equatorial speed of 8.55 km s^{-1}, whereas the projected rotation of Aa indicates $V \sin i \sim 27$ km s^{-1}. Hence, the radius of Aa is 3.2 $R_\odot$ or larger. This component is obviously evolved. The *Gaia* DR2 assigns a radius of 3.24 $R_\odot$ and the effective temperature of 5440 K, treating this object as a single star. The standard relations for main sequence stars do not apply to this system and, consequently, the masses and temperatures of the components can be only guessed. Here, $T_{\rm eff}$ of 5080, 5900, and 5900 K are assumed corresponding to spectral types K0, G0, and G0.

The combined V magnitude and the relative fluxes estimated from the areas of the CCF dips (with a small correction for the dependence of the CCF area on the assumed effective temperature) lead to the relative fluxes of Aa, Ab, and B of of 0.61, 0.23, and 0.16 and the individual V magnitudes 8.92, 9.97, and 10.35 mag, respectively. The *Gaia* DR2 parallax of 6.851±0.063 mas defines the absolute magnitudes, assuming zero extinction. The individual $V-K$ colors of the components are not measured directly; I assume here the $V-K$ colors of 2.2, 1.6, and 1.5 mag that match the combined K magnitude; however, this is just a guess constrained by the combined $V-K$ color. Figure 13 (b) shows the location of the components on the CMD (the absolute magnitudes M_V are measured, while the $V-K$ colors are guessed). For reference, two isochrones from Dotter et al. (2008) for the age of 10 Gyr and two values of [Fe/H] are plotted.

Considering the isochrones, the components of HIP 111598 are old and, likely, moderately metal-poor stars (see below), while their masses are close to 1 $M_\odot$. They are located near the main sequence turn-off: Aa has expanded while Ab and B are still close to the main sequence. No attempt of a quantitative match with isochrones is made here because the knowledge of metallicity and individual colors (or temperatures) is still lacking (the turn-off mass depends on the age and metallicity). The luminosities and assumed effective temperatures correspond to the stellar radii of 3.2, 1.3, and 1.1 $R_\odot$.

In principle, the spectra of individual components can be determined and modeled using spectral disentangling

[4] Codebase: https://doi.org/10.5281/zenodo.321854

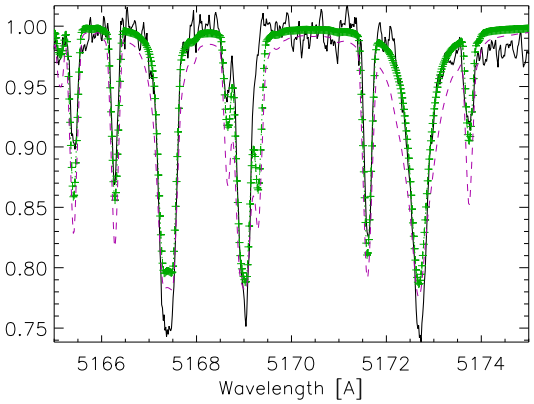

FIG. 14.— Fragment of the disentangled spectrum of HIP 111598 Ab (full line) is compared to the synthetic spectra with $T_e = 5900$ K, $\log g = 3.5$, [Fe/H]=−0.5 dex (green line and crosses) and [Fe/H]=0 (magenta dash) in the region around Mg Ib triplet. The synthetic spectra are scaled for the relative flux of 0.25 to account for the dilution by other components. Both spectra are smoothed by a 4 km s^{-1} boxcar. The lack of pressure broadening in strong lines suggests a low gravity and a sub-solar metallicity.

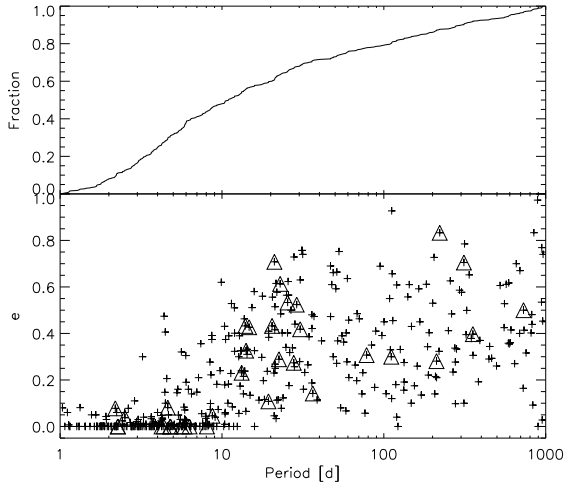

FIG. 15.— Period-eccentricity relation for inner subsystems in solar-type hierarchies from the MSC. Orbits from papers 1–6 of this series are marked by triangles. The upper plot is the cumulative distribution of periods.

(Hadrava 2009). However, this procedure is not straightforward, computationally intensive, and designed for binaries rather than triples; moreover, the author is not an expert in this field. To isolate the spectrum of one component, I use the normalized spectra with merged echelle orders and take advantage of the measured RVs. The spectra are co-added with centering on the selected component, while the moving features of other components are washed out by averaging. Using these initial co-added spectra of the components as a first guess, the result is refined iteratively by subtracting contributions of all components except one, shifting and averaging again. The disentangled spectrum of the sharp-lined component Ab is compared in Figure 14 with the synthetic spectra form Palacios et al. (2010)[5] with the effective temperature of 5900 K, $\log g = 3.5$, solar and sub-solar metallicity. The agreement is not very good, with some lines being stronger and some other weaker. Synthetic spectra with $\log g = 4.5$ or with solar metallicity have wider lines and do not match the observed spectrum of Ab.

If the mass sum of Aa and Ab is $\sim$2 $M_\odot$, the inner orbital radius is 17 $R_\odot$ and the Roche radius of the component Aa is about 7 $R_\odot$, so this binary is still detached. The absence of eclipses constrains the inner inclination to $i_{\rm Aa,Ab} < 78\overset{\circ}{.}5$. The orbital inclinations cannot be evaluated without reliable mass estimates. However, the similarity of the inner spectroscopic mass sum, $M_{\rm Aa+Ab} \sin^3 i_{\rm Aa,Ab} = 1.62\ M_\odot$, and the outer primary mass $M_{\rm Aa+Ab} \sin^3 i_{\rm A,B} = 1.49\ M_\odot$, suggests that the orbital inclinations can be similar. Therefore, the inner and outer orbits could be quasi-coplanar.

This compact triple system is rather unusual in several respects. First, one expects the components in the close 5.9 day binary to rotate synchronously with the orbit. The large star Aa indeed rotates almost synchronously, as evidenced by the photometric period. However, the less evolved star Ab has narrow lines corresponding to $V \sin i \approx 4.5$ km s^{-1}, whereas the synchronous equatorial speed of a star with $R = 1.3 R_\odot$ is 11 km s^{-1}. Either Ab indeed rotates slowly or its axis has a small inclination, hence is misaligned with the orbit. In both cases, rapid tidal alignment is expected. Therefore, this triple system has acquired its present-day architecture only recently. Another unusual characteristic of this system is its rather short outer period of 271 d. Such compact triple systems are rare, and they are predominantly coplanar (Borkovits et al. 2016).

This system appears to be relatively old, as suggested by the large radius of the star Aa and the absence of the 6707Å lithium line. Its spatial velocity $(U, V, W) = (10.7, -12.4, -30.8)$ km s^{-1} is typical for Galactic disk population. The high chromospheric activity of Aa is likely caused by its synchronization with the orbit. The slow rotation of B, $V \sin i = 1.9$ km s^{-1}, also suggests an old age. However, in an old close binary the component Ab should also be synchronized with the orbit, which is not the case here.

The semimajor axis of the outer pair A,B is 6 mas, so it can be resolved with long-baseline interferometers. Accurate astrometry of the outer pair can reveal the orientation of the inner orbit (its semimajor axis is 0.6 mas), defining the true mutual inclination in this interesting system. *Gaia* should detect photocentric motion of the star, as its estimated amplitude is about 2.5 mas. In fact, the goodness-of-fit parameter `gofAL` in *Gaia* DR2 is large, 10.08, indicating the detection of the astrometric signal. Brandt (2018) derived a highly significant acceleration of $(-0.6, +1.4)$ mas yr^{-1}.

4. SUMMARY

Historically, close subsystems in visual binaries were discovered photometrically (by eclipses) and then often followed spectroscopically. This produced a strong bias favoring short periods. Figure 1 of Tokovinin & Smekhov (2002) shows a sharp drop in the number of inner subsystems with $P > 7$ d known at the time. However, their own work on spectroscopic orbits resulted in a more uniform period distribution. The maximum at $P < 7$ d was interpreted as a signature of Kozai-Lidov cycles with tides, in agreement with the distribution expected from the population synthesis (Fabrycky & Tremaine 2007; Hamers 2019).

Nowadays the situation has changed dramatically be-

[5] See http://pollux.oreme.org.

cause most known subsystems in solar-type hierarchies were discovered spectroscopically (by variable RVs or double lines) rather than photometrically. This method works in a much wider range of inner periods. Unknown orbital elements of spectroscopic subsystems discovered from a few spectra, e.g. by Nordström et al. (2004), are determined by the follow-up work, including this series of papers.

Figure 15 shows the period-eccentricity plot for 528 inner subsystem with primary mass less than 1.5 $M_\odot$ extracted from the MSC. The 36 orbits resulting from this series (a modest 7% of the total) are highlighted by the triangles. The cumulative distribution of periods is also plotted. Quite remarkably, this curve shows no details suggesting a local maximum at $P \sim 10$ d. Instead, this distribution is smooth. Of course, the sample extracted from the MSC is biased, being derived from heterogeneous sources. However, the lack of the tidal signature in the period distribution is obvious.

The preference of close binaries to be inner members of hierarchical systems is a well established fact. Overall, the statistics of hierarchical multiplicity in the 67-pc sample of solar-type stars matches independent combination of inner and outer periods selected from the same distribution and filtered by the dynamical stability criterion. However, this model does not work for subsystems with $P < 10$ d because their number is larger than would result from an independent selection (see Fig. 11 in Tokovinin 2014). Therefore, formation of close binaries within hierarchies is somehow enhanced, but is not necessarily related to tides.

An alternative channel of close binary formation is the inward migration of wider pairs driven by accretion. In this case, the presence of outer companion(s) is, on one hand, a consequence of the accretion (availability of the mass supply sufficient to form additional companions) and, on the other hand, a factor that might help migration by supplying mis-aligned gas to the inner binary. Mass ratios of accreting binaries always increase and often tend asymptotically toward one (twins). Indeed, many inner subsystems studied here are twins.

I thank the operator of the 1.5-m telescope R. Hinohosa for executing observations of this program and L. Paredes for scheduling and pipeline processing. Comments by the Referee, K. Fuhrmann, helped to improve the manuscript.

This work used the SIMBAD service operated by Centre des Données Stellaires (Strasbourg, France), bibliographic references from the Astrophysics Data System maintained by SAO/NASA, and the Washington Double Star Catalog maintained at USNO. This work has made use of data from the European Space Agency (ESA) mission *Gaia* (https://www.cosmos.esa.int/gaia), processed by the *Gaia* Data Processing and Analysis Consortium (DPAC, https://www.cosmos.esa.int/web/gaia/dpac/consortium). Funding for the DPAC has been provided by national institutions, in particular the institutions participating in the *Gaia* Multilateral Agreement.

Facility: CTIO:1.5m

REFERENCES

Borkovits, T., Hajdu, T., Sztakovics, J,, et al. 2016, MNRAS, 455, 4136
Boro Saikia, S., Marvin, C. J., Jeffers, S. V. et al. 2018, A&A, 616, 108
Brandt, T. D. 2018, ApJS, 239, 31
Desidera, S., Gratton, R. G., Lucatello, S. et al. 2006, A&A, 454, 553
Dotter, A., Chaboyer, B., Jevremović, D. et al. 2008, ApJS, 178, 89
Eker, Z., Filiz Ak, N., Bilir, S. et al. 2008, MNRAS, 389, 1722
Evans, D. S. 1968, QJRAS, 9, 388
Fabrycky D. & Tremaine S., 2007, ApJ, 669, 1298
Fekel, F. C. 1981, ApJ, 246, 879
Fuhrmann, K. & Chini, R. 2019, MNRAS, 482, 471
Gaia Collaboration, Brown, A. G. A., Vallenari, A., Prusti, T. et al. 2018, A&A, 595, 2 (Vizier Catalog I/345/gaia2).
Gomez, J., Docobo, J. A., Campo, P. P. & Mendez, R. A. 2016, AJ, 152, 216
Guillout, P., Klutsch, A., Frasca, A. et al. 2009, A&A, 504, 829
Hadrava, P. 2009, A&A, 494, 399
Hamers, A. 2019, MNRAS, 482, 2262
Jenkins, J. S., Díaz, M., Jones, H. R. A. et al. 2015, MNRAS, 453, 1439
Kiraga M., 2012, Acta Astron., 62, 67
Mason, B. D., Wycoff, G. L., Hartkopf, W. I., Douglass, G. G. & Worley, C. E. 2001, AJ, 122, 3466 (WDS)
Moe, M. & Kratter, K. M. 2018, ApJ, 854, 44
Nordstrom, B. & Andersen, J. 1985, A&AS, 61, 53
Nordström, B., Mayor, M., Andersen, J. et al. 2004, A&A, 418, 989
Palacios A. , Gebran M., Josselin E. et. al 2010, A&A, 516, 13
Plavchan, P., Werner, M. W., Chen, C. H. et al. 2009, ApJ, 698, 1068
Pojmanski, G., 1997, Acta Astronomica, 47, 467.
Tokovinin, A. AJ, 2014, 147, 87
Tokovinin, A. 2015, AJ, 150, 177
Tokovinin, A. 2016a, AJ, 152, 11 (Paper 1)
Tokovinin, A. 2016b, AJ, 152, 10 (Paper 2)
Tokovinin, A. 2016c, ORBIT: IDL Software for Visual, Spectroscopic, and Combined Orbits, Zenodo, doi:10.2581/zenodo.61119
Tokovinin, A. 2017, ORBIT3Orbits of Triple Stars, Zenodo, doi:10.5281/zenodo.321854
Tokovinin, A. 2018a, ApJS, 235, 6
Tokovinin, A. 2018b, AJ, 156, 48 (Paper 3)
Tokovinin, A. 2018c, AJ, 156, 194 (Paper 4)
Tokovinin, A. 2019, AJ, 157, 91 (Paper 5)
Tokovinin, A., Corbett, H., Fors, O., et al. 2018, AJ, 156, 120
Tokovinin, A., Fischer, D. A., Bonati, M. et al. 2013, PASP, 125, 1336
Tokovinin, A. & Latham, D. W. 2017, ApJ, 838, 54
Tokovinin, A., Mason, B. D., Mendez, R. A. et al. 2019, AJ, 158, 48
Tokovinin, A., Pribulla, T., & Fischer, D. 2015, AJ, 149, 8
Tokovinin, A. A. & Smekhov, M. G. 2002, A&A, 382, 118
van Leeuwen, F. 2007, A&A, 474, 653 (HIP2)